The Journal of Immunology

RESEARCH ARTICLE | JANUARY 15 2016

The Fractalkine-Receptor Axis Improves Human Colorectal Cancer Prognosis by Limiting Tumor Metastatic Dissemination FREE

Marco Erreni; ... et. al

J Immunol (2016) 196 (2): 902–914.
https://doi.org/10.4049/jimmunol.1501335

The Fractalkine-Receptor Axis Improves Human Colorectal Cancer Prognosis by Limiting Tumor Metastatic Dissemination

Marco Erreni,* Imran Siddiqui,*,[1] Giulia Marelli,*,[1] Fabio Grizzi,[†] Paolo Bianchi,[†] Diego Morone,* Federica Marchesi,*,[‡] Giuseppe Celesti,[†] Samantha Pesce,* Andrea Doni,* Cristiano Rumio,[§] Massimo G. Roncalli,[¶,‖] Luigi Laghi,*,[†] Alberto Mantovani,*,[¶] and Paola Allavena*

Human colorectal cancer (CRC) is a frequent neoplasia in Western countries, and its metastatic progression is a major cause of cancer-related death. In search of specific molecules upregulated in CRC, with possible clinical relevance, we performed a differential gene-profiling analysis in surgery-derived CRC samples and adjacent uninvolved intestinal mucosa. The chemokine CX_3CL1 and its specific receptor CX_3CR1 were significantly upregulated in tumors. Higher expression of CX_3CL1 and CX_3CR1 was confirmed by immunohistochemistry in 100 CRC tumor samples (stages I–III). Unexpectedly, high immune scores of CX_3CL1 did not correlate with the density of tumor-infiltrating $CD3^+$ T cells or $CD68^+$ macrophages. Coexpression of ligand and receptor by tumor cells (axis-positive tumors) significantly associated with longer disease-free ($p = 0.01$) and disease-specific survival ($p = 0.001$). Conversely, axis-negative tumors (with low expression of both ligand and receptor) had increased risk of tumor relapse ($p = 0.02$), and increased likelihood of metachronous metastasis ($p = 0.001$), including after stage adjustment ($p = 0.006$). Transduction of CX_3CL1 and CX_3CR1 in CRC tumor cell lines induced cell aggregation that strongly inhibited in vitro migration in chemotaxis assays. In a mouse model of spleen–liver metastases, cancer dissemination to liver was dramatically reduced in CX_3CL1-CX_3CR1–expressing tumors, and ligand–receptor interaction was confirmed in cancer cells in vivo by fluorescence resonance energy transfer analysis. In conclusion, tumoral expression of the CX_3CL1-CX_3CR1 chemokine axis functions as a retention factor, increasing homotypic cell adhesion and limiting tumor spreading to metastatic sites. Lack or low levels of expression of CX_3CL1-CX_3CR1 by tumor cells identifies a group of CRC patients at increased risk of metastatic progression. *The Journal of Immunology*, **2016, 196: 902–914.**

Colorectal cancer (CRC) is a frequent malignancy and still a major cause of cancer-related death. Major advances have defined the genetic alterations and molecular pathways involved in tumor progression (1, 2). Recent studies highlighted that alteration of the intestinal barrier and penetration of commensal microbiota triggers innate immune cells and initiates an inflammatory response (3–5). It is now established that an inflammatory microenvironment plays a major role in cancer development (6, 7). In CRC, this evidence is even stronger and is supported by the epidemiological findings that neoplastic transformation is more frequent in patients with inflammatory bowel disease and that long-term treatment with nonsteroidal anti-inflammatory drugs has a protective role (8). Sustained expression of transcription factors (e.g., NF-κB, STAT3) and inflammatory mediators (e.g., cyclooxygenase 2, cytokines: IL-6, IL-23, chemokines) links chronic inflammation and tumorigenesis (9, 10). As far as the adaptive immunity is concerned, host–tumor interactions have emerged as a pivotal factor in CRC progression: the increasing density of tumor-infiltrating lymphocytes has been documented as being positively associated with improved overall as well as disease-free survival (11–14). However, this holds true only for early-stage tumors, as in some studies this association was lost in cancers with nodal metastasis (12). A better understanding of the biological features and diversity of this neoplasia in terms of clinical outcome is needed.

In a differential gene-profiling analysis between freshly isolated human CRC samples and autologous adjacent uninvolved intestinal mucosa, we found many differentially expressed genes (15): among these, the chemokine CX_3CL1 and its specific receptor CX_3CR1 were selected for further investigation. Unlike other

*Department of Immunology and Inflammation, Humanitas Clinical and Research Center, 20089 Rozzano, Milan, Italy; [†]Laboratory of Gastroenterology, Humanitas Clinical and Research Center, 20089 Rozzano, Milan, Italy; [‡]Department of Medical Biotechnology and Translational Medicine, University of Milan, 20133 Milan, Italy; [§]Department of Pharmacology and Biomolecular Science, University of Milan, 20133 Milan, Italy; [¶]Humanitas University, 20089 Rozzano, Milan, Italy; and [‖]Department of Pathology, Institute for Clinical Care and Scientific Research Humanitas Clinical and Research Center, 20089 Rozzano, Milan, Italy

[1]I.S. and G.M. contributed equally to this study.

ORCID: 0000-0002-5688-1009 (G.M.).

Received for publication June 12, 2015. Accepted for publication November 12, 2015.

This work was supported by Italian Association for Cancer Research Investigator Grants (to P.A. and A.M.), Italian Ministry of Universities and Research FIRB Grant RBAP11H2R9 (to A.M.), and Humanitas Clinical and Research Center Translation in Medical Oncology Grant 2013 (to F.M.). I.S. was supported by a Marie Curie fellowship via the Initial Training Network Grant Advanced Teaching and Training for Adoptive Cell Therapy. M.E. was supported by a fellowship from Fondazione Umberto Veronesi.

Address correspondence and reprint requests to Dr. Paola Allavena and Dr. Marco Erreni, Laboratory of Cellular Immunology, Humanitas Clinical and Research Center, Via Manzoni 113, 20089 Rozzano, Milan, Italy. E-mail addresses: paola.allavena@humanitasresearch.it (P.A.) and marco.erreni@humanitasresearch.it (M.E.)

The online version of this article contains supplemental material.

Abbreviations used in this article: CRC, colorectal cancer; DFS, disease-free survival; DSS, disease-specific survival; ECM, extracellular matrix; EGFP, enhanced GFP; FLIM, fluorescence lifetime imaging microscopy; FRET, fluorescence resonance energy transfer; HR, hazard ratio; OR, odds ratio; PFA, paraformaldehyde; $rhCX_3CL1$, human recombinant CX_3CL1; RT, room temperature.

family members, CX_3CL1 (originally named Fractalkine) is a *trans*-membrane chemokine that can be cleaved by specific proteases (16, 17). It is expressed at low levels by several cell types (neurons, endothelial, and epithelial cells) and is induced by inflammatory stimuli (IL-1, TNF, IFN-γ). CX_3CL1 is involved in the pathogenesis of different inflammatory/autoimmune conditions (18, 19). Overexpression of CX_3CL1 and/or its receptor CX_3CR1 was described in different human tumors (20–24) and was associated with immune cell infiltration (25, 26) and tumor cell invasion (21, 27). In particular, expression of the CX_3CL1-CX_3CR1 axis in tumors has been associated with increased metastatic capacity, directing the tropism of circulating cancer cells to bones (20). Moreover, our group demonstrated that CX_3CR1 overexpression is an early event in pancreatic cancer progression and correlates with tumor invasion of local nerves and ganglia (21, 23).

In this study, we report that coexpression of CX_3CL1 and its receptor CX_3CR1 by neoplastic cells is significantly associated with more favorable patients' prognosis. Conversely, low expression of both molecules identifies a subset of patients with significantly higher risk of developing distant metastasis and rapid tumor progression.

Materials and Methods

Patients and tissue specimens

Patients included in this study underwent resective surgery for colorectal cancer at the Clinical and Research Institute Humanitas (Milan, Italy) from 1997 to 2003. The absence of metastasis at diagnosis was assessed by combining histopathological findings, surgical records, and perioperative imaging. Postsurgical tumor recurrence was monitored by thoracoabdominal computerized tomography, abdominal ultrasonography, and chest radiography. The study was approved by the Institute Ethical Committee, and written informed consent was obtained from patients.

Abs and reagents

The following Abs were used: mouse anti-human CD68 (Dako), mouse anti-human CD3 (Dako), rabbit anti-human CX_3CR1 (Abcam), goat anti-human CX_3CL1 (R&D Systems), mouse anti-human β_4-integrin (Abcam), mouse anti-human β_1-integrin (R&D Systems), mouse anti-human $\alpha_V\beta_5$ integrin (R&D Systems), rabbit anti-human CX_3CL1 (Torrey Pines Biolabs), rat anti-mouse F4/80 (Serotec), rat anti-mouse CD3 (eBioscience), Alexa donkey anti-goat 647, Alexa donkey anti-rabbit 488, Alexa donkey anti-mouse 647, Alexa goat anti-rabbit 647, Alexa goat anti-rabbit 488 (Invitrogen), biotin-conjugated donkey anti-goat (SantaCruz Biotecnology), ABC Vectastain, and HRP rabbit/mouse Envision (ChemMate, Dako). Cells were transfected with Lipofectamine (Invitrogen). Human recombinant CX_3CL1 ($rhCX_3CL1$) was from R&D Systems. Where required, Tyramide Signal Amplification Systems (PerkinElmer) has been used.

Immunohistochemistry

Formalin-fixed, paraffin-embedded, and 2-μm–thin sections of tumor samples were deparaffinized and exposed or not to an Ag-retrieval system, before being incubated with the specific Ab. Endogenous peroxidase activity was blocked with 3% hydrogen peroxide for 20 min at room temperature (RT). Primary Ab was applied for 1 h at RT. Reactive sites were identified by exposure to a HRP-conjugated secondary Ab for 30 min at RT. Immunoperoxidase staining was then obtained by using diaminobenzidine as a chromogen (DAB+chromogenX-50, ChemMate; DakoCytomation, Carpinteria, CA). The slides were finally counterstained with hematoxylin (Harris Hematoxilyn, DiaPath, Microstain Division, Martinengo, Bergamo, Italy). Immunostaining of CX_3CL1 and CX_3CR1 in tumor samples was evaluated by three independent operators, blind to any patient clinical data. Scores of CX_3CL1 and CX_3CR1 expression by tumor cells were calculated considering the percentage of positive tumor cells and staining intensity classified as negative (0), moderate (1), and strong (2). For each specimen, the entire section was analyzed and the final score was calculated using the following formula:

$$\frac{(0\times\%\text{ of negative tumor cells})+(1\times\%\text{ of moderate tumor cells})+(2\times\%\text{ of strong tumor cells})}{100}$$

$CD3^+$ and $CD68^+$ cell density at the tumor invasive margin was measured in three randomly selected and noncontiguous microscopic areas encompassing the deep front of tumor invasion. For each selected area, the cancer tissue had to represent ~50% of the entire microscopic field. The pathologist who selected the areas was blinded to any patient clinical data. For each selected region, a digital image was captured. A computer-aided image analysis software was used, able to discriminate the immunostained area on the basis of RGB color segmentation, and to calculate the percentage of immunoreactive area as a fraction of the total area digitally captured.

Animal experiments

Eight-week-old female nude mice (purchased form Charles River), NSG mice (purchased from The Jackson Laboratory), and $CX_3CR1^{gfp/gfp}$ mice (purchased from The Jackson Laboratory) were used for mouse models. Animals were maintained in a specific pathogen-free facility. Procedures involving animals and their care conformed to institutional guidelines in compliance with national (4D.L. N.116, G.U., suppl. 40, 18-2-1992) and international law and policies (European Economic Community Council Directive 2010/63/EU, OJ L 276/33, 22.09.2010; National Institutes of Health *Guide for the Care and Use of Laboratory Animals*, U.S. National Research Council, 2011). All efforts were made to minimize the number of animals used and their suffering. Nude mice (10 mice per group) received a s.c. injection into the flank with 2×10^6 viable cells. Tumors were measured every 3 d by caliper. After 1 mo, mice were sacrificed, and tumors were removed and used for subsequent experiments.

NSG mice were used for the spleen–liver model of metastasis. Eight-week-old female NSG mice were anesthetized, and the spleen was exposed through a left lateral flank incision. Tumors were established by intrasplenic injection of 2×10^6 cells in suspension using a 27-gauge needle. The injection site on the spleen was pressed with a cotton stick to wipe out any spilled cells and ensure hemostasis. The peritoneum and skin were closed with surgical thread. After the indicated period, mice were sacrificed, and spleen and liver were removed and used for subsequent analysis. The experiment was repeated four times, for a total of 80 mice used. The percentage of metastatic area was analyzed using VS120-S5 Virtual Slide System (Olympus) and ImagePro Analyzer 7.0 (Media Cybernetics).

$CX_3CR1^{gfp/gfp}$ and sex-matched $CX_3CR1^{+/gfp}$ mice were used for azoxymethane/dextran sodium sulfate model of colitis-associated cancer. Briefly, mice were weighted and given a single i.p. injection of azoxymethane (10 mg/kg). Seven days later, animals received 3% dextran sulfate sodium in drinking water. Colon cancer was induced after three cycles of dextran sulfate sodium treatment, which consisted of 6 d of 3% dextran sulfate sodium, followed by 2 wk of normal drinking water. After 70 d, mice were sacrificed, and colon was collected, fixed in 4% paraformaldehyde (PFA), and embedded within OCT.

Immunofluorescence

Cell lines were cultured on glass slides coated with poly-L-lysine, washed in PBS, and fixed in 4% PFA for 15 min at RT. DAPI (Invitrogen, Molecular Probes) was used to stain nuclei. Slides were mounted with Fluor Preserve Reagent (Calbiochem) and analyzed with confocal microscope. Frozen sections were fixed in 4% PFA for 15 min at RT. After two washes in 2% bovine albumin serum (BSA) in PBS, tissues were incubated with the specific primary Ab and diluted in 2% BSA, 0.1% Triton X-100, 0.1% glycine, 5% normal donkey, or goat serum in PBS. After three washes in washing buffer (0.2% BSA, 0.05% Tween 20 in PBS), tissues were incubated with specific secondary Ab for 1 h at RT. After four washes in washing buffer, DAPI was used to stain nuclei. Tissues were mounted with Fluor Preserve Reagent (Calbiochem) and analyzed with confocal microscope. All the images were acquired with a laser-scanning confocal microscope (FluoView FV1000; Olympus). For image analysis, Imaris ×64 7.0.2 Software (Bitplane, AG) was used.

Cell culture

Cells were cultured in RPMI 1640 medium supplemented with 10% FCS (Lonza, BioWhittaker) and 2 mM Ultraglutamine1 (Lonza, BioWhittaker) and routinely tested for mycoplasma contamination.

Lentiviral infection

The lentiviral vector pRRL.sinPPT.CMV.CX_3CR1-enhanced GFP (EGFP) containing CX_3CR1-EGFP chimera under the promoter of CMV was a gift from M.L. Malosio, Institute of Neuroscience, Consiglio Nazionale delle Ricerche, Milan, Italy, and Humanitas Clinical and Research Center. This vector was used to substitute the EGFP with cDNA encoding mCherry and the CX_3CL1-mCherry chimera. Briefly, CX_3CL1 and CX_3CR1 were cloned by RT-PCR amplification of cDNA isolated from DLD-1 cells and human monocytes, respectively. The full-length

cDNAs of CX_3CL1 and CX_3CR1 were cloned into pmCherry-N1 and pEGFP-N1 (Clontech), respectively. CX_3CL1 and CX_3CR1 TGA stop codon were deleted to generate Cherry- or GFP-fusion proteins. For CX_3CL1, XhoI and BamHI restriction enzymes were used. For CX_3CR1, HindIII and BamHI restriction enzymes were used. For CX_3CL1 cloning, the following primers were used: 5′- CCGCTCGAACCATGGCTCCGATATC-3′ and 5′-CGGGATCCCGCACGGGCACCAGGAC-3′. For CX_3CR1, the following primers were used: 5′- CCCAAGCTTGGGATGGATCAGTTCCCTGAATC-3′ and 5′- CGGGATCCCGGAGAAGGAGCAATGCATCTC-3′. To generate lentiviral vector, EGFP, CX_3CR1-GFP, CX_3CL1-cherry, and pmCherry inserts were cut from pEGFP-N1 or pmCherry-N1, respectively, and cloned into the lentiviral vector.

Lentiviruses were produced by transfecting the 293T cell line (plated at a density of 750,000 cells per 10-cm–diameter dish 3 d before) with the packaging plasmid (pCMV-ΔR8.74), the envelope plasmid (containing *VSV-G* gene), and 10 μg DNA of interest. Supernatants were collected 48 h after transfection, filtered (0.45 μm), and used to infect cells. After the addition of 5 μl polybrene, 5 ml of each supernatant was added to cells, plates were centrifuged for 1 h at 900 rpm (acceleration 3, breaking 0), and then incubated in a humified atmosphere of 5% CO_2 and 95% air at 37°C. Supernatants were removed after 24 h, and a second cycle of infection was repeated. After 48 h, cells were cultured in RPMI 1640 medium supplemented with 10% FBS (Lonza, BioWhittaker) and 2 mM Ultraglutamine1 (Lonza, BioWhittaker). Infected cells were selected based on GFP or Cherry fluorescence.

Intracellular calcium^{2+} influx

Intracellular calcium^{2+} influx was measured with Fura-2. Briefly, cells were plated on glass-bottom culture dishes (MatTek). After 24 h, cells were treated with 0.1 μM Fura-2 (Invitrogen) diluted in DMSO for 30 min. Subsequently, cells were incubated in a humidified atmosphere of 5% CO_2 and 95% air at 37°C and monitored with a Cell-R IX81 microscopy (Olympus). At the indicated time point, 100 ng/ml rhCX_3CL1 was added, and the variation in Fura-2 emission at 340 and 380 nm was analyzed in a time-lapse experiment (one image every 3 s) for the indicated time. Calcium^{2+} influx was measured as ratio between Fura-2 emission at 340 and 380 nm (340/380 ratio).

Migration assay

Migration assay was performed in 24-well Transwell plates (Corning), with inserts of 8.0-μm pore size. Infected cells were mixed at a 1:1 ratio, to generate axis-positive (CX_3CL1^{cherry}-CX_3CR1^{gfp}) or axis-negative tumors ($mock^{cherry}$-$mock^{gfp}$). Cells were resuspended in RPMI 1640 medium with 1% FCS at 10^6 cells/ml; 200 μl cell suspension was loaded in the upper chamber of the Transwell, and 600 μl medium was loaded in the lower chamber: where indicated, 10% FCS or different concentrations of rhCX_3CL1 were added. After 16 h, migrating cells were counted, analyzing 20–30 fields per filter. Results express migrated cells/field. Alternatively, cells were stained with Crystal Violet. Subsequently, crystals were disrupted with 10% acetic acid, and the absorbance of this solution was read at 595 nm.

Adhesion assay

Adhesion assay to extracellular matrix (ECM) was performed using ECM Cell Adhesion Array Kit, colorimetric from Millipore. Briefly, RKO- or NCI-H630–infected cells were cocultured to generate axis-positive (CX_3CL1^{cherry}-CX_3CR1^{gfp}) or axis-negative ($mock^{cherry}$-$mock^{gfp}$) tumors: cells were let to adhere for 30 min, and, subsequently, assay was performed as manufacturer's instructions.

For adhesion assay on cell monolayers, CX_3CL1^{cherry} or $Mock^{cherry}$ cells were plated on glass slides coated with poly-L-lysine in 24-well plates (Costar) and cultured to confluence. CX_3CR1^{gfp} or $Mock^{gfp}$ cells were resuspended at the concentration of 4×10^5 cells/ml in adhesion medium (RPMI 1640, 1% FCS, 2 mM Ultraglutammine1, 0.5% BSA), and 500 μl was plated in each well and incubated for 20 min in a humidified atmosphere of 5% CO_2 and 95% air at 37°C, with gentle shaking. After two washes with PBS to remove nonadherent cells, slides were fixed with 4% PFA, mounted with Fluor Preserve Reagent (Calbiochem), and analyzed with confocal microscope. For each sample, different fields were analyzed, and GFP^+ cells were counted. Alternatively, GFP^+ cells were counted by flow cytometry. Where indicated, cells were pretreated (overnight) with pertussis toxin, *Bordetella pertussis* (Calbiochem), or corresponding Ab to block integrin activity (1 h).

RT-PCR and quantitative real-time PCR

Total RNA was isolated using TRI reagent (Ambion) and quantified by Nanodrop. DNase treatment (Turbo DNA-free kit; Ambion) was performed to avoid genomic DNA contamination. A quantity amounting to 1 μg total RNA was reverse transcribed using the High-Capacity cDNA Archive kit (Applied Biosystems), according to the manufacturer's instructions. cDNA was analyzed by SYBR Green–based quantitative real-time PCR on ABI Prism 7900HT Fast Real Time PCR System (Applied Biosystem). The 18S was used as internal control to normalize. All gene-specific primers were designed in-house. The sequences of primers are as follows: CX_3CL1 forward, 5′-TCTGCCATCTGACTGTCCTG-3′ and reverse, 5′-TGATGTTGCATTTCGTCACA-3′; CX_3CR1 forward, 5′-GGGACTGTGTTCCTGTCCAT-3′ and reverse, 5′-GACACTCTTGGGCTTCTTGC-3′; ITGB1 forward, 5′-GTGGAGGAAATGGTGTTTGC-3′ and reverse, 5′-CGTTGCTGGCTTCACAAGTA-3′; ITGB4 forward, 5′-ATCCCCATCTTTGCTGTCAC-3′ and reverse, 5′-ATGTTGGACGAGTCCTCCTG-3′; ITGB5 forward, 5′-GGTTGGGATTTGGGTCTTTT-3′ and reverse, 5′-GGACGCAATTTGGAAACAAC-3′; 18S forward, 5′-CGCCGCTAGAGGTGAAATTC-3′ and reverse, 5′-CTTTCGCTCTGGTCCGTCTT-3′.

In vitro proliferation assay

Cells were counted and resuspended at a concentration of 10^3 cells/ml. A total of 100 μl cell suspension was plated into 96-well plates. Cell proliferation has been measured after 4 h to set the starting conditions, then after 1, 3, 5, and 7 d. A total of 20 μl MTT (5 mg/ml in 1× PBS) was added to each well (200 μl medium) and left at 37°C for 2–4 h, in the dark. After aspiration of the medium, 100 μl DMSO was added to each well and crystals were dissolved by pipetting. The absorbance of this solution was measured at 570 nm.

Fluorescence resonance energy transfer

Fluorescence resonance energy transfer (FRET) analysis was performed by fluorescence lifetime imaging microscopy (FLIM), using the Trimscope II two-photon microscope (LaVision Biotec, Bielefeld, Germany). FLIM measurements were obtained illuminating the sample with a Chameleon Ultra II laser (Coherent, CA) with 80 MHz repetition rate tuned at 830 nm for two-photon excitation. Fluorescence emission was detected with FLIM ×16-78 Mhz TCSCP Detector (LaVision BioTec). Measurements were performed on the confocal system previously described with a 20× water immersion objective (XLUMPlanFLn, numerical aperture 1.0; Olympus). FRET efficiency (E) was obtained by calculating the different lifetime distributions in the phasor plots and then using the formula $E = 1 - \tau_{DA}/\tau_D$, where τ_{DA} is the donor fluorescence lifetime in presence of the acceptor and τ_D is the donor fluorescence lifetime alone. The distance between the two molecules was calculated as $R_0\ (1/E - 1)^{1/6}$, where R_0 is the Föster radius (5.1 nm) relative to GFP-cherry couple. Acquisition and instrument control was performed using Imspector Pro software (LaVision, BioTec), whereas data analysis was performed with Prism (GraphPad).

Statistical analysis

Student's *t* test, nonparametric Mann–Whitney *U* test, parametric one-way or two-way ANOVA (with Tukey's or Sidak's posttest, respectively), nonparametric Kruskal–Wallis (with Dunn's posttest), linear and logistic regression analysis, and Cox proportional hazard model (univariate and multivariate analysis) were used as indicated. Survival rates were estimated by the Kaplan–Meier method and compared with the log-rank test. Analyses were done using Epi Info version 3.4.3 and GraphPad Prism6.

Results

Expression of CX_3CL1 in human CRCs and lack of correlation with leukocyte infiltration

Results from a transcriptional profiling of surgically resected human CRC samples, performed with an Inflammation Array (Applied Biosystems), indicated that the chemokine ligand CX_3CL1 was overexpressed in tumors, compared with the normal adjacent colonic mucosa. Validation experiments demonstrating upregulated CX_3CL1 in a series of 27 CRC specimens are shown in Supplemental Fig. 1A. Protein expression was further investigated by immunohistochemistry in 18 normal colonic tissues, 18 adenomas, and 100 colorectal cancer tissues (stages I–III). All carcinoma samples were genotyped as microsatellite stable. Immunoreactivity was scored considering staining intensity and the percentage of positive tumor cells (as detailed in *Materials and Methods*). CX_3CL1 was expressed by healthy colonic epithelial

cells, and its expression was progressively increased in precancerous lesions and early stage tumors (Fig. 1). Notably, CX_3CL1 expression was highly heterogeneous and in stage III tumors it significantly decreased compared with stage I (Fig. 1B).

Given the established role of CX_3CL1 in recruiting immune cells at inflamed sites, we investigated whether tumor expression of CX_3CL1 was responsible for immune cell infiltration, which importantly impacts on disease outcome (28, 29). In the same case list of tumor samples, the density of $CD3^+$ lymphocytes and $CD68^+$ macrophages was scored at the tumor invasive margin (Fig. 2A). Based on the median values of the immune reactive area, CRC samples were divided as high or low infiltrated. Surprisingly, linear regression analysis showed no association between CX_3CL1 immunoscore and $CD3^+$ or $CD68^+$ cell density (CD3: $r^2 = 0.003$, $p = 0.61$; CD68: $r^2 = 0.003$ $p = 0.56$; Fig. 2B, 2C), even after tumor stratification by stage (Supplemental Fig. 1B–D), indicating that CX_3CL1 expressed by tumor cells is not directly responsible for leukocyte recruitment in colorectal tumors. In line with this finding, although in healthy colonic mucosa the majority of immune cells was CX_3CR1 positive, in tumor tissues only a limited number of infiltrating cells recruited at the tumor front expressed the receptor (Fig. 2D). Using immunofluorescence, we also observed that only very few $CD3^+$ or $CD68^+$ tumor-infiltrating cells were CX_3CR1 positive (Fig. 2E).

This finding was confirmed in a mouse model of colon carcinogenesis, using $CX_3CR1^{+/gfp}$ and $CX_3CR1^{gfp/gfp}$ mice, which feature a disruption of the *CX3CR1* exon 2 by *EGFP* insertion in one or both alleles, respectively. As the CX_3CR1 receptor is predominantly expressed by monocytes and gut-resident macrophages, this model was specifically used to track the recruitment of myeloid cells expressing or not CX_3CR1 in tumor tissues. In $CX_3CR1^{gfp/gfp}$ mice lacking the receptor, $F4/80^+$ macrophages and $CD3^+$ lymphocytes abundantly infiltrated the tumor and their density was even significantly increased in comparison with receptor-competent mice ($CX_3CR1^{+/gfp}$) (Fig. 2F, 2G). In these mice, leukocytes recruited at the tumor front did not express CX_3CR1, and the very few spots of colocalization are shown in Fig. 2F. Overall, these data strongly support the conclusion that the CX_3CL1-CX_3CR1 axis is not

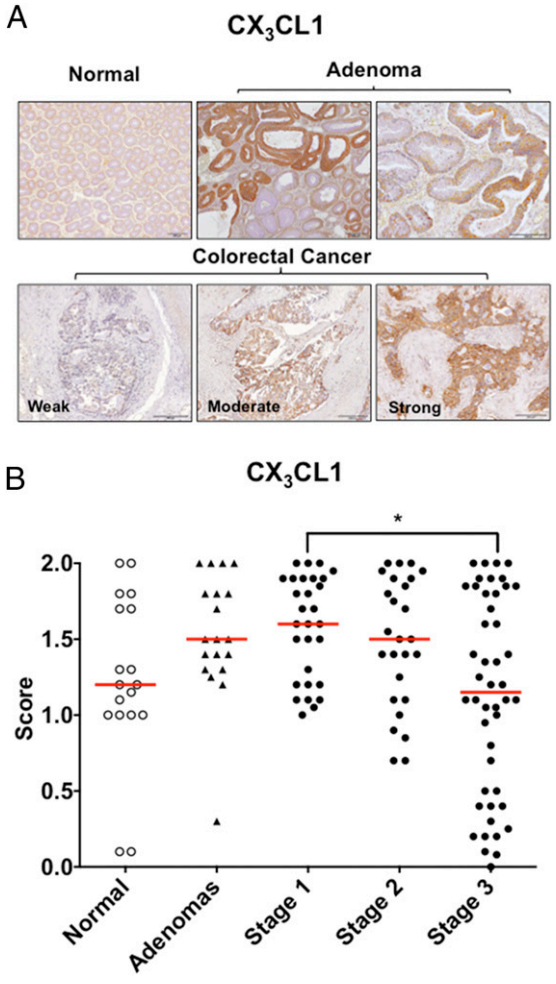

FIGURE 1. Immunohistochemical analysis of CX_3CL1 expression in human colorectal cancer. (**A**) Representative immunoreactivity of CX_3CL1 in normal colonic mucosa, precancerous lesion (adenoma), and colorectal cancer. Original magnification ×20. (**B**) Expression scores of CX_3CL1 in all tested samples (normal colonic mucosa, $n = 18$; adenoma, $n = 18$; colorectal cancer, $n = 100$). CX_3CL1 increases in adenoma and carcinoma, but decreases in stage III tumors. Red bars indicate median value. Kruskal–Wallis and Dunn's posttest, $*p < 0.05$.

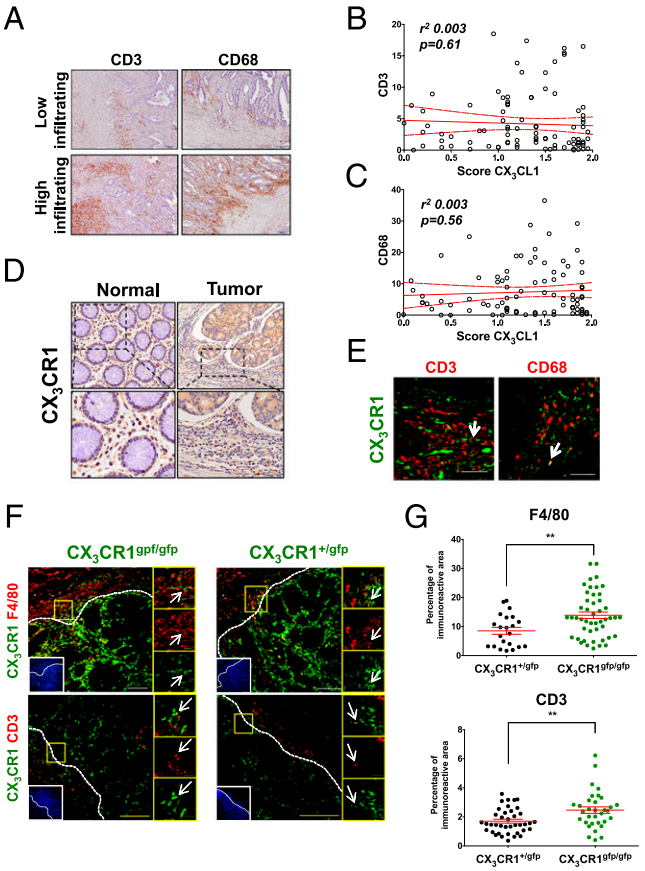

FIGURE 2. CX_3CL1 expression by tumor cells does not correlate with $CD3^+$ or $CD68^+$ infiltrating cells at the tumor invasive front. (**A**) Immunohistochemical analysis of $CD3^+$ or $CD68^+$ cells in CRC samples ($n = 100$), at the tumor-invasive margin. (**B** and **C**) Linear regression analysis. Correlation between CX_3CL1 expression and the percentage of $CD3^+$ (B) or $CD68^+$ (C) cells. CX_3CL1 expression does not correlate with lymphocyte or macrophage infiltration. (**D**) Immunohistochemistry of CX_3CR1 showing that in tumor tissue only few immune-infiltrating cells express CX_3CR1, whereas in healthy mucosa the majority of immune cells are CX_3CR1 positive. (**E**) Immunofluorescence of CX_3CR1 and CD3 or CD68 in human tumor tissues; arrows mark the few double-positive cells. (**F**) Mouse model of colitis-associated cancer in $CX_3CR1^{gfp/gfp}$ and $CX_3CR1^{+/gfp}$ mice. Immunofluorescence of $CD3^+$ and $F4/80^+$ cells; arrows mark the few double-positive cells. White dotted lines indicate the margin of the tumor. Original magnification ×20. (**G**) Quantification of $F4/80^+$ and $CD3^+$ cell infiltration in tumor tissue. Student t test, $**p < 0.01$.

involved in the recruitment of lymphocytes and macrophages in colon cancer tissues.

Coexpression of CX_3CL1 and CX_3CR1 by tumor cells and relevance to patients' clinical outcome

Immunohistochemistry for CX_3CR1 revealed that also tumor cells stained positive for the receptor. Therefore, all 100 CRC samples were scored for CX_3CR1 immunostaining: whereas the receptor staining was faint in healthy colon and in precancerous lesions, in most carcinoma samples it was strongly expressed (Fig. 3A, 3B). Based on the median values of the immune reactive area for CX_3CL1 or CX_3CR1 expression, CRC samples were divided as high- or low-expressing tumors, and their phenotype was correlated with demographic and tumor pathological features (Supplemental Table 1). Interestingly, CX_3CL1 expression was inversely correlated with the occurrence of lymph node metastasis, both in univariate and multivariate analysis (odds ratio [OR] 0.29, $p = 0.003$, OR 0.23, $p = 0.002$, respectively). In addition, low expression of CX_3CL1 correlated with a significantly increased disease recurrence (indicated as disease-free survival [DFS], $p = 0.03$) and reduced patients' survival (indicated as disease-specific survival [DSS], $p = 0.04$) (Supplemental Fig. 1E, 1F). Similar results were found for CX_3CR1, even if the statistical analysis demonstrated significance only for DSS (DFS, $p = 0.08$; DSS, $p = 0.01$) (Supplemental Fig. 1G, 1H).

Next, we observed that one third of CRC samples (31.7%) coexpressed high levels of both CX_3CL1 and CX_3CR1, as shown in the example in Fig. 3C, which depicts several spots of colocalization in immunofluorescence. Based on median values, CRC specimens were classified as tumors with high coexpression of CX_3CL1 and CX_3CR1 (Lig^{High}-Rec^{High}, or axis-positive tumors), and tumors with low coexpression (Lig^{Low}-Rec^{Low}, or axis-negative tumors), and tumors with single positivity (Lig^{Low}-Rec^{High} ; Lig^{High}-Rec^{Low}). Kaplan–Meier curves showed that patients with Lig^{Low}-Rec^{Low} tumors (axis-negative tumors) had significantly worse DFS and DSS, compared with positive Lig^{High}-Rec^{High} tumors or with single-positive tumors (log rank, $p = 0.01$ and $p = 0.001$, respectively, Fig. 3D, 3E). Results of the Cox Proportional Hazard model also showed that patients with axis-negative tumors had significantly higher risk of relapse (hazard ratio [HR] 2.59, $p = 0.02$), as well as of specific death (HR 5.95, $p = 0.006$). Adjusting the model for tumor stage, patients with axis-negative tumors had a close to significant risk of disease progression (DFS, HR 2.2, $p = 0.07$) and a significant risk of tumor-related death (DSS, HR 3.7, $p = 0.04$) (Table I). In addition, axis-negative tumors were associated with a significantly increased occurrence of lymph node metastasis (logistic regression: univariate, OR 1.58, $p = 0.02$; multivariate, OR 5.01, $p = 0.01$) (Table II) and increased likelihood of developing metachronous metastasis (logistic regression, OR 10.5, $p = 0.001$), even after stage adjustment (logistic regression, OR 8.03, $p = 0.006$) (Fig. 4A) (Table III). Overall, the results indicated that CRC tumors nonexpressing the ligand–receptor axis had significantly higher frequency of disease recurrence and metastasis.

We next investigated ligand–receptor expression by tumor cells at metastatic sites. Among the 46 stage III patients in our case list, we analyzed all available corresponding lymph node metastatic samples (36 patients). We compared, within the same patients,

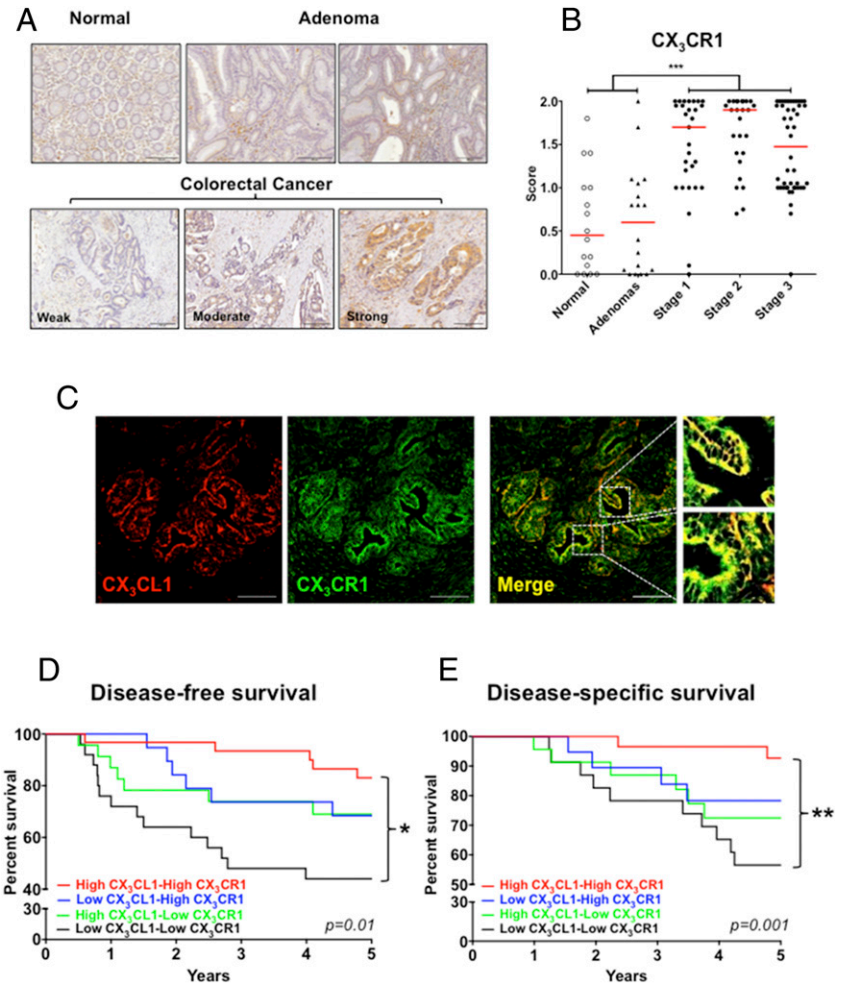

FIGURE 3. Immunohistochemical analysis of CX3CR1 expression in human CRC and correlation of the CX_3CL1-CX_3CR1 axis with clinical outcome. (**A**) Representative immunoreactivity of CX_3CR1 in normal colonic mucosa, precancerous lesion (adenoma), and colorectal cancer. Original magnification ×20. (**B**) Expression scores of CX_3CR1 in all tested samples (normal colonic mucosa, $n = 18$; adenoma, $n = 18$; colorectal cancer, $n = 100$). CX_3CR1 is low in normal tissues and precancerous lesions, and strongly increases in tumors. Kruskal–Wallis and Dunn's posttest, $***p < 0.001$. (**C**) Immunofluorescence analysis showing the coexpression of CX_3CL1 (red) and CX_3CR1 (green) on tumor cells. The presence of several spots of colocalization is shown in the merge panel and close-up. Original magnification ×20. (**D** and **E**) Kaplan–Meier curves showing disease-free (D) and disease-specific (E) survival, in stage I–III patients according to CX_3CL1-CX_3CR1 axis expression. Patients with axis-negative tumors (Lig^{Low}-Rec^{Low}, black line) have significantly shorter DFS and DSS ($p = 0.01$ and $p = 0.001$, respectively), compared with axis-positive tumors (Lig^{High}-Rec^{High}, red line).

Table I. Predictive factors for DFS and DSS in patients with stage I–III CRC

		DFS				DSS			
		Univariate		Stage Adjustment		Univariate		Stage Adjustment	
Variables		HR (95% CI)	*p*	HR (95% CI)	*p*	HR (95% CI)	*p*	HR (95% CI)	*p*
Age[a]		1.41 (0.72–2.78)	0.3	1.02 (0.99–1.05)	0.3	1.58 (0.68–3.7)	0.29	1.02 (0.98–1.06)	0.34
Sex (male)		0.59 (0.3–1.16)	0.13	0.59 (0.3–1.16)	0.13	0.43 (0.18–1.03)	0.06	0.48 (0.2–1.16)	0.1
Tumor site	Distal	1.0		1.0		1.0		1.0	
	Proximal	0.44 (0.19–1.05)	0.07	0.5 (0.21–1.2)	0.12	0.53 (0.18–1.59)	0.26	0.64 (0.21–1.94)	0.43
	Rectum	1.09 (0.51–2.3)	0.8	1.19 (2.5–0.56)	0.65	1.41 (0.55–3.65)	0.48	1.42 (0.55–3.67)	0.47
Local tumor invasion[b]	T1[c]	1.0		1.0		—			
	T2[d] (T1-T2)[l]	0.46 (0.04–5.13)	0.53	0.26 (0.02–-4.18)	0.34	1.0		1.0	
	T3[e]	3.5 (0.48–25.75)	0.22	0.4 (0.01–12.2)	0.5	12.3 (92.1–1.65)	0.01	1.61 (0.21–12.1)	0.65
	T4[f]	4.9 (0.57–42.08)	0.15	0.54 (0.02–13)	0.73	20.6 (184.8–2.3)	0.007	2.06 (0.23–18.5)	0.52
Lymph node metastasis		2.54 (1.30–4.9)	0.006	—		10 (2.99–33.6)	<0.001	—	
Tumor cell type	ADC[g]	1.0		1.0		1.0		1.0	
	Variant[h]	2.26 (0.79–6.39)	0.13	1.36 (0.46–4.01)	0.58	2.38 (0.71–7.99)	0.16	1.39 (0.41–4.77)	0.6
Vascular invasion		2.08 (1.05–4.08)	0.03	1.37 (0.66–2.8)	0.39	3.6 (1.62–8.03)	0.002	1.85 (0.81–4.24)	0.14
Grading[i]	G1-G2[j]	1.0		1.0		1.0		1.0	
	G3[k]	2.04 (0.89–4.67)	0.09	1.27 (0.53–3.04)	0.59	3.86 (1.6–9.36)	0.003	1.64 (0.66–4.05)	0.29
CX_3CL1-CX_3CR1 loop	Positive-axis tumors	1.0		1.0		1.0		1.0	
	High CX_3CR1–Low CX_3CL1	1.07 (0.39–2.96)	0.89	0.95 (0.34–2.68)	0.92	2.4 (0.54–10.8)	0.25	1.65 (7.43–0.37)	0.52
	High CX_3CL1–Low CX_3CR1	1.15 (0.44–3.01)	0.78	1.34 (0.51–3.56)	0.55	3.23 (0.81–12.9)	0.1	3.55 (14.3–0.88)	0.07
	Negative-axis tumors	2.59 (1.15–5.86)	0.02	2.2 (0.95–5.14)	0.07	5.95 (1.66–21.4)	0.006	3.7 (13.4–1.02)	0.04

Cox proportional hazard model. An HR <1.0 (a reference point) represents a decreased likelihood of DFS or DSS, whereas a HR >1.0 represents increased likelihood.
[a]Age entered as continuous variables.
[b]Local tumor invasion.
[c]T1, tumor invading submucosa.
[d]T2, invading muscolaris propria.
[e]T3, invading through the muscolaris propria.
[f]T4, invading adjacent organs or perforating visceral peritoneum.
[g]Adenocarcinoma.
[h]Mucinous histology, medullary type.
[i]Tumor differentiation.
[j]G1–G2, well-to moderate differentiated cancer.
[k]G3, poorly differentiated cancer.
[l]In DSS Cox regression, T1 and T2 tumors were grouped due to the lack of death events in T1 tumors.

Table II. Correlation between CX_3CL1-CX_3CR1 axis and demographic and tumor pathological features

		CX_3CL1-CX_3CR1 Expression		Univariate Analysis		Multivariate Analysis	
		High (32)	Low (25)	OR (95% CI)	*p*	OR (95% CI)	*p*
Age	Years, mean ± SD	66.5 ± 11.5	61.4 ± 13.2	0.97 (0.93–1.01)			
Sex	Male	16	20	1.0		1.0	
	Female	16	5	0.63 (0.42–0.94)	0.02	0.19 (0.05–0.72)	0.01
Tumor site	Distal	10	8	1.0			
	Proximal	11	11	1.25 (0.36–4.36)	0.73		
	Rectum	11	6	0.68 (0.17–2.66)	0.58		
Tumor site	T1	3	1	1.0			
	T2	9	3	1 (0.07–13.6)	1.0		
	T3	19	19	3 (0.29–31.4)	0.36		
	T4	1	2	6 (0.2–162.4)	0.29		
Lymph node metastasis	No	22	9	1.0		1.0	
	Yes	10	16	1.58 (1.1–2.28)	0.02	5.01 (1.47–17.2)	0.01
Tumor cell type	ADC	31	24	1.0			
	Variant	1	1	1.09 (0.43–2.79)	0.86		
Vascular invasion	No	25	18	1.0			
	Yes	7	7	1.12 (0.75–1.67)	0.59		
Grading	G1–G2	31	21	1.0			
	G3	1	4	1.81 (0.85–3.84)	0.12		

Logistic regression analysis. Positive-axis tumors and negative-axis tumors were correlated with patients' clinical and pathological features. OR <1.0 represents a decreased relationship between CX_3CL1-CX_3CR1 axis and the considered variables, whereas OR >1.0 (a reference point) represents an increased relationship.

CI, confidence interval.

expression in primary tumors and in metastatic lymph nodes; in metastatic tumor cells, both CX_3CL1 and CX_3CR1 expression was significantly reduced (Fig. 4B–D). The finding that tumor cells at metastatic sites have lower expression of the ligand–receptor axis suggests that negative cells may be more prone to disseminate, possibly because the missing membrane-bound CX_3CL1 or its cognate receptor cannot engage anymore in an adhesion loop.

The CX_3CL1-CX_3CR1 axis mediates increased homotypic cell adhesion

To gain insights into the adhesive mechanism of this chemokine axis and its potential in counteracting cell mobility, we generated CX_3CL1- or CX_3CR1-transduced human cells. From eight CRC cell lines screened, we selected the RKO cell line (negative for both ligand/receptor) and the NCI-H630 cell line (receptor-negative but expressing low levels of membrane-bound CX_3CL1; Supplemental Fig. 2A). Cells were separately infected with CX_3CL1^{cherry} or with CX_3CR1^{gfp} fusion genes, or with corresponding empty vectors ($mock^{cherry}$ and $mock^{gfp}$) (Supplemental Fig. 2B). Receptor-expressing cells showed rapid calcium flux (Supplemental Fig. 2C) and enhanced migration in response to $rhCX_3CL1$ (Supplemental Fig. 2D), confirming proper functionality.

In adhesion assays, CX_3CR1 cells indeed had increased adherence to monolayers of ligand-expressing cells (Fig. 5A, Supplemental Fig. 2E). Furthermore, when receptor/ligand-transduced cells were cocultured at 1:1 ratio (to mimic axis-positive tumors), chemotaxis in response to $rhCX_3CL1$ or FBS gradients was abrogated, as cells formed large aggregates that prevented migration through filter pores (Fig. 5B–D, Supplemental Fig. 2F). Thus, receptor–ligand interaction among neoplastic cells effectively results in a sufficiently strong adhesive engagement that prevents tumor cell migration in response to an otherwise strong chemoattractant stimulus.

In different contexts (e.g., leukocytes and endothelial or neuron cells), CX_3CL1-mediated recruitment of CX_3CR1^+ cells can be either integrin dependent or not (30, 31). We therefore investigated integrin involvement in the CX_3CL1-CX_3CR1–mediated adhesion among tumor cells. Both RKO and NCI-H630 cells are positive for β_1 and β_5 integrins and negative for β_3 and β_6 integrins, whereas β_4 is strongly expressed only in NCI-H630 cells (Supplemental Fig. 3A). When cells were cocultured to mimic axis-positive or -negative tumors, integrin expression was not modulated at the mRNA (Supplemental Fig. 3B) or protein level (Supplemental Fig. 3C). Adhesion of CX_3CR1^{gfp} cells on monolayers of CX_3CL1^{cherry} cells was not affected in the presence of blocking anti-β1 and anti-β5 mAbs (Fig. 5E). Similarly, adhesion to ECM-coated plates was identical in axis-positive or -negative cocultured cells, and anti-β1 mAb equally reduced adhesion on collagen-coated plates (data not shown). Furthermore, when CX_3CR1-expressing cells were pretreated with pertussis toxin, to block G protein signaling, the increased adhesion to CX_3CL1 cell monolayer was not significantly reduced (Fig. 5F). Overall, we conclude that the homotypic adhesion between receptor/ligand-expressing cells is both integrin and G protein signaling independent.

As chemokines may affect tumor cell growth and CX_3CL1 has been implicated in sustaining cell proliferation via activation of the epidermal growth factor pathway (32), we next investigated whether transduced cells had different proliferative patterns in vitro and in vivo. Neither the ligand nor the receptor did affect the in vitro growth of RKO and NCI-H630 cells, even when receptor/ligand-positive cells were cocultured (i.e., CX_3CL1^{cherry} + CX_3CR1^{gfp}) (Supplemental Fig. 3D). When injected s.c. in vivo in immune-deficient mice, all cell combinations formed stably growing tumors, which, however, did not differ in size among the groups (Supplemental Fig. 3E). Thus, the presence of a functional CX_3CL1-CX_3CR1 chemokine axis had no impact on tumor cell proliferation in vitro and in vivo.

CX_3CL1-CX_3CR1–mediated homotypic cell adhesion reduces tumor cell metastatic potential in vivo

Based on the evidence in CRC patients that low or absent expression of this chemokine axis was associated with higher risk of developing metastases, we next investigated the metastatic potential of our transduced cells. These tumor cell lines do not spontaneously metastasize when grown in vivo; therefore, a spleen–liver model of metastasis was set up. Combinations of positive-axis (CX_3CL1^{cherry} + CX_3CR1^{gfp}) or negative-axis ($mock^{cherry}$ + $mock^{gfp}$) RKO tumor cells were injected in the spleen of NSG mice. After 18 d, the overall survival of mice was

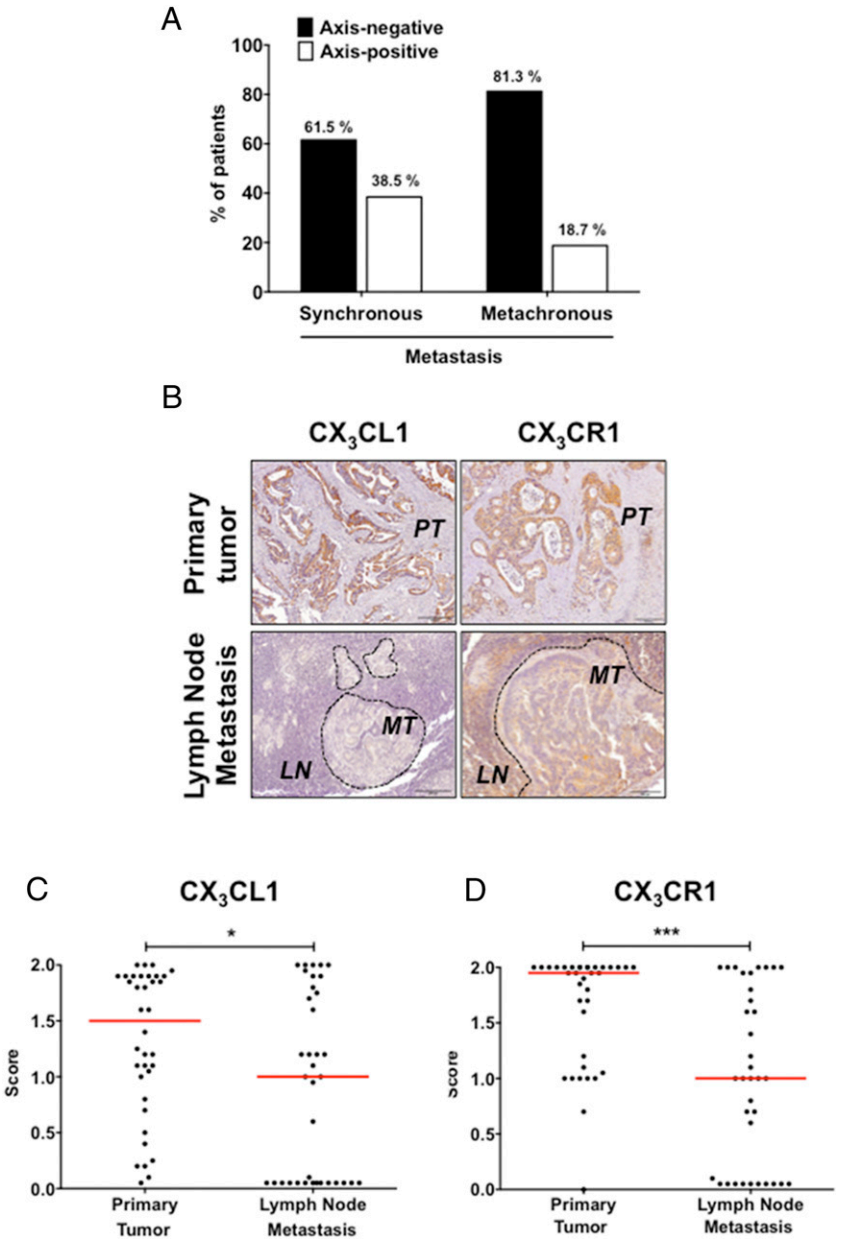

FIGURE 4. CX_3CL1 and CX_3CR1 expression is reduced in lymph node metastasis. (**A**) Percentage of patients with lymph node metastasis at diagnosis and with metachronous metastasis (during follow-up), according to the expression of the chemokine axis by tumor cells. Patients with axis-negative tumors (Lig^{Low}-Rec^{Low}) have higher frequency of metastases compared with axis-positive tumors (Lig^{High}-Rec^{High}). (**B**) Immunoreactivity of CX_3CL1 and CX_3CR1 in lymph node metastases and corresponding primary tumors. Original magnification ×20. (**C** and **D**) Expression scores of CX_3CL1 (C) and CX_3CR1 (D) in lymph node metastases (n = 36) and primary tumors (n = 36). Red bars indicate median value. Expression of both CX_3CL1 and CX_3CR1 in metastatic cells is significantly reduced. Mann–Whitney, $*p < 0.05$, $***p < 0.001$. LN, lymph node; MT, metastatic tumor; PT, primary tumors.

dramatically different in the two groups, with only 2 of 10 mice bearing negative tumors alive, compared with 8 of 10 mice with positive-axis tumors (Fig. 6A). In a shorter experiment (12 d), negative-axis tumors developed many more metastases (area 22.57%) compared with positive tumors (area 5.08%; $p < 0.001$) (Fig. 6B, 6C). Single-positive tumors were also tested: whereas $mock^{cherry}$-CX_3CR1^{gfp}-RKO cells generated several metastases, cells expressing only the ligand (i.e., CX_3CL1^{cherry}-$Mock^{gfp}$) had less metastases, yet more than positive-axis tumors ($p < 0.01$) (Fig. 6B, 6C), most likely because of the "sticky" nature of the chemokine ligand. Comparable results were obtained with NCI-H630 cells, which have an epithelial phenotype and when spleen injected developed liver metastasis only after 40 d: axis-negative tumors again showed a dramatic increase in the metastatic area (8.5%) compared with axis-positive tumors (0.19%) ($p < 0.01$) (Fig. 6B, 6D). Of note, the combination of CX_3CR1^{gfp}-$Mock^{cherry}$ cells also produced less metastases ($p < 0.05$). This finding is consistent with the endogenous expression of CX_3CL1 in this cell line, sufficient to establish a functional CX_3CL1-CX_3CR1 loop (Fig. 6B, 6D). Overall, these results demonstrate that ligand–receptor interaction among tumor cells leads to strong homotypic adhesion that results in reduced tumor cell metastatic potential in vivo.

FRET analysis of the CX_3CL1-CX_3CR1 interaction in vivo

To confirm a direct interaction between CX_3CL1 and CX_3CR1 in vivo, we performed FLIM/FRET analysis. Sections were obtained from axis-positive or -negative tumors grown in mouse spleens (both RKO and NCI-H630 cells), and 5–10 different regions of GFP and Cherry coexpression were selected (Fig. 7A). FLIM images in the phasor plot representation (33) (Fig. 7B, 7C) showed a shift-down in GFP fluorescence lifetime only in axis-positive tumors (Fig. 7B, 7C, red square), indicating a quenching and thus the presence of FRET events. By comparing the corresponding different GFP fluorescence lifetime (green square versus red square) in axis-positive tumor phasor plots, we found a significant reduction in GFP mean lifetime ($p < 0.001$) (Fig. 7D, 7E); from these data, we calculated the efficiency of FRET (E) and the mean distance R between GFP and Cherry proteins (that corresponds to the distance between CX_3CL1 and CX_3CR1). Of note, comparable values of E and R were obtained in both RKO and

Table III. Likelihood of metachronous metastasis according to CX_3CL1-CX_3CR1 axis status

CX_3CL1-CX_3CR1 Axis Status	Metachronous Metastasis		Univariate		Stage-Adjusted	
	No (75)	Yes (25)	OR (95% CI)	*p*	OR (95% CI)	*p*
Positive-axis tumors	29	3	1.0		1.0	
High CX_3CR1–Low CX_3CL1	16	4	2.42 (0.48–12.2)	0.28	1.75 (0. 3–9.36)	0.5
High CX_3CL1–Low CX_3CR1	18	6	3.2 (0.7–14.5)	0.13	3.7 (0.7–18.1)	0.1
Negative-axis tumors	12	13	10.5 (2.5–43.5)	0.001	8.03 (1.8–35.3)	0.006

Logistic regression: an OR >1.0 (a reference point) represents an increased likelihood of developing metachronous metastasis.
CI, confidence interval.

NCI-H630 axis-positive tumors. These results confirmed that a molecular interaction between CX_3CL1 and CX_3CR1 indeed occurs in vivo.

Discussion

In this study, we have shown that CRC patients whose tumor cells coexpress the chemokine CX_3CL1 and its receptor CX_3CR1 have a more favorable prognosis, and, conversely, low expression of both molecules significantly associates with an increased risk of disease progression. In particular, the CX_3CL1-CX_3CR1 axis seems to play an important role in preventing the metastatic process, because patients having axis-negative tumors showed a dramatic increased risk of developing metachronous metastases. Our experimental results in vitro and in vivo with ligand/receptor-transduced CRC cell lines provide evidence that CX_3CL1-CX_3CR1 interaction increases adhesiveness among tumor cells and limits their motility and dissemination. This interpretation is supported by the following findings: 1) CX_3CR1^+ cells have enhanced adherence on cell monolayers expressing the ligand; 2) cells coexpressing both CX_3CR1 and CX_3CL1 form aggregates and fail to migrate in vitro; 3) in a mouse model in vivo, CX_3CL1^+-CX_3CR1^+ tumors have lower metastatic potential; 4) FRET/FLIM analysis demonstrated direct ligand–receptor interaction in tumors growing in vivo. Therefore, both patients' and experimental findings indicate that, if neoplastic cells within the primary mass lose this chemokine axis, they are less engaged and free to spread and give metastasis. Of note, a clear-cut statistical significance was found only when considering tumors double negative for ligand and receptor, versus double-positive tumors. Tumors with single positivity, only expressing either the

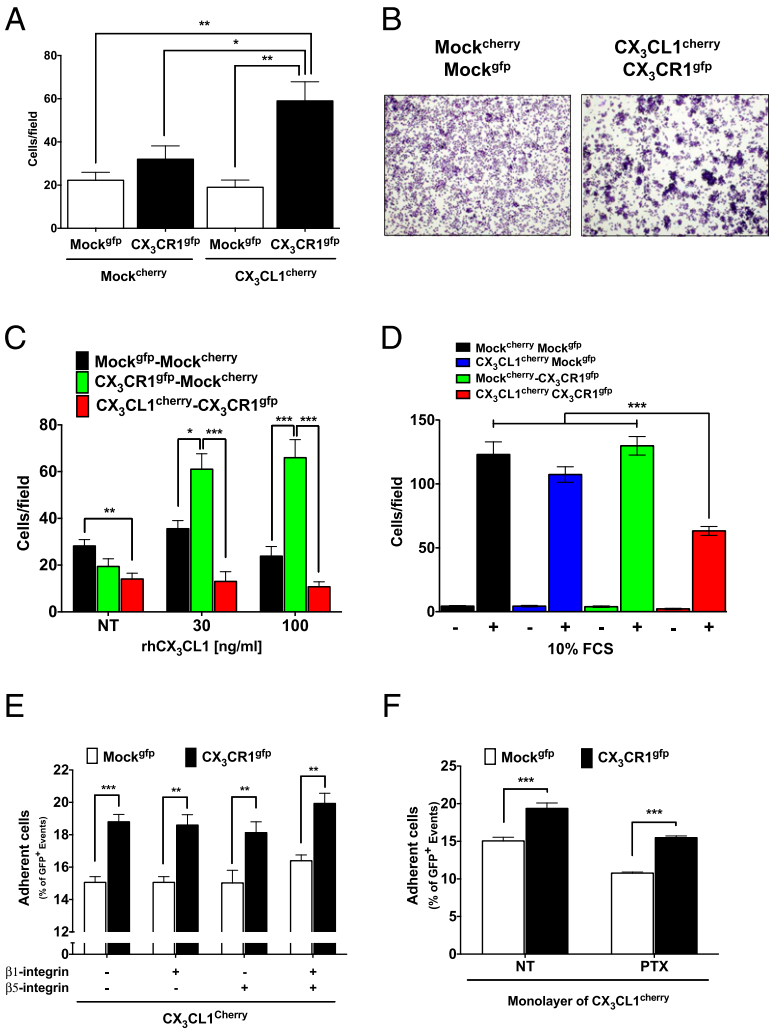

FIGURE 5. Expression of the chemokine axis CX_3CL1-CX_3CR1 increases homotypic cell–cell adhesion and inhibits tumor cell migration in vitro. (**A**) Adhesion assay on monolayers of RKO CX_3CL1^{cherry} or $Mock^{cherry}$ cells. RKO cells expressing CX_3CR1^{gfp} show significantly increased adhesion on CX_3CL1 monolayers compared with $Mock^{gfp}$ cells. (**B**) Enhanced aggregation of RKO cells when cocultured to mimic axis-positive (CX_3CL1^{cherry}-CX_3CR1^{gfp}) compared with axis-negative ($Mock^{cherry}$-$Mock^{gfp}$) tumors. (**C** and **D**) Chemotaxis assay of cocultured RKO cells. Migration is inhibited in cocultures of axis-positive cells (red bars) in response to rhCX_3CL1 (C) or 10% FCS (D) due to large cell aggregates. (**E**) Role of integrins in the enhanced adhesion of RKO CX_3CR1^{gfp} cells on monolayer of RKO CX_3CL1^{cherry} cells. Anti-β_1 and anti-β_5 integrin-blocking Abs do not affect adhesion of CX_3CR1 cells on CX_3CL1 monolayers. (**F**) Cell pretreatment with pertussis toxin (PTX) did not alter the increased adhesion of CX_3CR1^{gfp} cells to CX_3CL1-expressing cell monolayers. Shown are representative experiments (3–4 replicates each), of at least three experiments, with similar results. One-way ANOVA with Tukey's posttest (A, C, D, and E) and two-way ANOVA with Sidak's posttest (E), $*p < 0.05$, $**p < 0.01$, $***p < 0.001$.

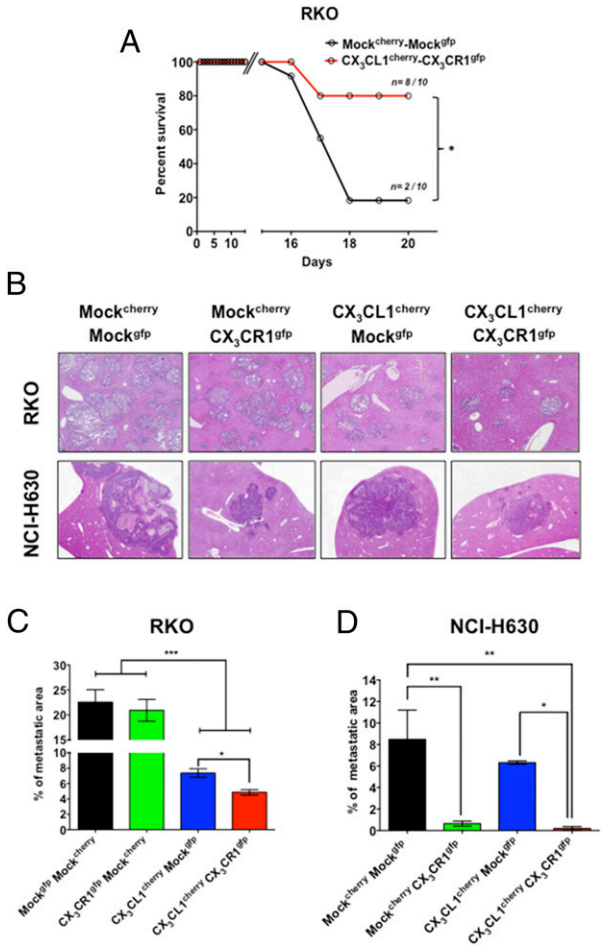

FIGURE 6. Expression of the chemokine axis CX_3CL1-CX_3CR1 reduces metastatic cell dissemination in vivo. In vivo spleen–liver mouse model of metastasis. NSG mice were spleen injected with 1:1 mixture of tumor cells expressing CX_3CL1 or CX_3CR1 or Mock cells (n = 10 mice each group). (**A**) Mice with axis-negative tumors ($Mock^{cherry}$-$Mock^{gfp}$, black line), had higher mortality rate compared with axis-positive tumors (CX_3CL1^{cherry}-CX_3CR1^{gfp}, red line). Log rank, $*p < 0.05$. (**B**) Representative histological pictures of liver metastasis from mice receiving different combinations of CX_3CL1^{cherry}- or CX_3CR1^{gfp}-expressing tumor cells (*upper panels*, RKO cells; *lower panels*, NCI-H630). Original magnification ×10. (**C** and **D**) Analysis of the liver metastatic area (mean ± SE of three experiments with RKO, one with NCI-H630). Mice with axis-negative tumors (black bars) had higher number of metastasis compared with axis-positive tumors (red bars). In (D), NCI-H630 cells constitutively produce low levels of CX_3CL1, and exogenous expression of CX_3CR1 reconstituted the chemokine axis, resulting in fewer metastases (green bar). One-way ANOVA with Tukey's posttest, $*p < 0.05$, $**p < 0.01$, $***p < 0.001$.

receptor (or the ligand), have a slightly increased risk of recurrence, but not statistically significant; this observation suggests that a low expression of ligand or receptor (below the median value) may, at least in some cases, be sufficient to engage the adhesive loop.

In homeostatic conditions, the chemokine CX_3CL1 is expressed at low levels in the gut and regulates the physiological recruitment of leukocytes (34); accordingly, a consistent proportion of resident intestinal intraepithelial and lamina propria leukocytes is CX_3CR1 positive (18, 35, 36). In neoplastic conditions, CX_3CL1 was upregulated in early stage CRC tumors, and already in preneoplastic lesions, but its expression decreased in advanced metastatic tumors. It is known that CX_3CL1 is induced by inflammatory cytokines such as TNF, IL-1, and IFN-γ (18, 35); its cellular localization is regulated by TNF, which activates specific proteases that cleave CX_3CL1 from the plasma membrane (37); in addition, TGF-β, whose expression correlates with CRC progression (38), suppresses its production (27). These observations suggest that the up- and downregulation of CX_3CL1 along CRC progression may be initially mediated by the presence of inflammatory cytokines and, at later stages, by increased protease and TGF-β activity. In addition, CX_3CL1 cleavage from the cell membrane can be modulated by androgens (20, 39); in our case list of patients, we found that loss of ligand, and therefore low expression of the CX_3CL1-CX_3CR1 axis, was more frequent in males than females, suggesting a possible role of sex hormones in reducing the membrane expression of CX_3CL1.

Whether the transmembrane and soluble forms of the chemokine have different roles is an open issue. In murine models, the soluble form was more important for the recruitment of immune cells (40). In our study, we did not test CX_3CL1 constructs exclusively generating the soluble chemokine, but the Mock-transfected NCI-H630 cells, which express the membrane-bound chemokine without secreting the soluble form, were informative in the in vivo metastasis assay: the results showed that cells expressing the membrane form only had similar adhesive efficiency compared with the CX_3CL1-transduced counterpart, which also produces large amounts of the soluble ligand.

In line with this finding, a recent paper demonstrated that the membrane-bound chemokine establishes stronger adhesion with the receptor, compared with the soluble chemokine. By protruding out of the membrane and the glycocalix, the mucin stalk facilitates the availability and presentation of CX_3CL1 to the receptor; furthermore, the transmembrane domain generates a permanent aggregation of chemokine monomers, and the cytosolic domain ensures adhesive robustness by interacting with the cytoskeleton (41).

Previous studies focused on the role of CX_3CL1 expressed by the tumor in recruiting a variety of immune cells such as lymphocytes, macrophages, and NK cells, at neoplastic sites, and boosting of antitumor immune responses (25, 40, 42, 43), including CRC (26, 44). Although NK cell infiltration is very scarce in CRC (45), macrophages and lymphocytes are largely present: in particular, it is well established that $CD3^+$ T cell infiltration at the tumor-invasive margin has a protective role (12, 28). In our study, we found no correlation between CX_3CL1 expression by tumor cells and the density of $CD3^+$ or $CD68^+$ cells; accordingly, very few tumor-infiltrating leukocytes at the invasive margin expressed the receptor. Supporting the observation made in human samples, in the mouse model of colitis-associated cancer, a limited number of infiltrating leukocytes expressed CX_3CR1, especially in the peritumoral areas. Of note, a recent paper described that $CD68^+$ macrophages infiltrating human CRC expressed CX_3CR1, which was markedly increased in advanced patients (46). This discrepancy could be explained by the use of different anti-CX_3CR1 reagents and the fact that our case list of samples mostly comprised early stage tumors.

As far as the receptor expressed by tumor cells, its presence has not been previously described in CRC. The mechanism responsible for receptor upregulation in tumors is unclear. CX_3CR1 is not modulated in vitro by several cytokines (21), but recent studies suggested a role for hypoxia and NF-κB in receptor regulation in pancreatic cancer (47, 48), a finding that we did not confirm (21) (and data not shown).

We and others have reported on CX_3CR1 expression in different neoplasias, such as prostate, breast, and pancreatic cancer; hepatocellular carcinomas; and glioblastomas (20–23, 49, 50).

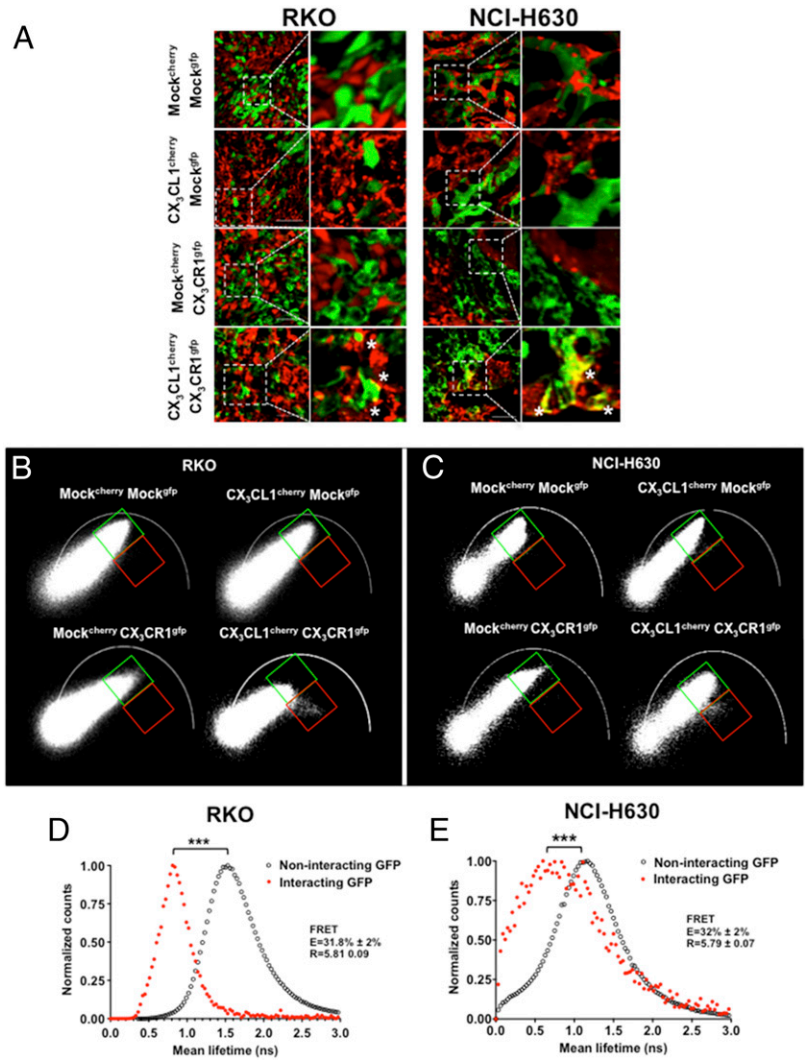

FIGURE 7. FRET analysis of CX_3CL1-CX_3CR1 interaction in vivo. (**A**) Immunofluorescence analysis of RKO (*left panel*) and NCI-H630 (*right panel*) tumors injected in mouse spleens. CX_3CL1-CX_3CR1 positive-axis tumors show several spots of colocalization (*inset*, white asterisk) that are absent in axis-negative tumors. Original magnification ×20. (**B** and **C**) Phasor plots were used to calculate GFP fluorescence lifetime variation in axis-positive or -negative tumors generated with RKO (B) or NCI-H630 (C) cells: a reduction in GFP fluorescence lifetime is present only in axis-positive tumors. Green boxes indicate normal GFP lifetime; red boxes indicate the reduced GFP lifetime. (**D** and **E**) FRET analysis of CX_3CL1-CX_3CR1 interaction. Comparison between mean lifetime of "interacting" versus "noninteracting GFP" in RKO (D) and NCI-H630 cells (E): starting from CX_3CL1^{cherry}-CX_3CR1^{gfp}–derived phasor plot, the mean lifetime of GFP, in the presence or absence of Cherry (interacting or noninteracting GFP, respectively), was compared. Interacting GFP shows a significantly lower fluorescence lifetime in comparison with noninteracting GFP, indicating the presence of FRET events and thus a CX_3CL1-CX_3CR1 interaction. Student *t* test, $***p < 0.001$.

There are contrasting results in the literature on the role of CX_3CR1 in the metastatic ability of tumor cells. In this manuscript, we have shown that CX_3CR1^+ tumor cells are retained within the primary tumor by homologous cells producing the ligand, and patients whose tumors coexpress both ligand and receptor have longer survival and lower risk of metastases. These results are in line with our previous observation in human pancreatic ductal adenocarcinoma, where we described that CX_3CR1^+ tumor cells adhere to nearby infiltrating neural cells and ganglia expressing CX_3CL1, and are preferentially associated to local, rather than distant, tumor recurrence (21). More recently, and in an independent cohort of patients, we reported that CX_3CR1 expression in pancreatic ductal adenocarcinoma is a feature of more differentiated (G1–G2) tumor cells, and is associated with better overall survival, in radically resected patients (23). In contrast, other studies reported that CX_3CR1^+ tumor cells, already circulating in the blood, are attracted at distant sites by other ligand-expressing cells. This is the case of prostate and breast cancer, where the ligand is produced by endothelial or stromal cells of the bone marrow, thus facilitating bone tropism and metastases (20, 50). The underlying mechanism is always the attraction of receptor-positive tumor cells by the chemokine, but the outcome can be dramatically different. In evaluating the role of CX_3CR1 in metastases, of major importance is to know whether the ligand is expressed within the primary tumor. If this is the case, then CX_3CR1^+ cells refrain from disseminating; if the ligand is absent, tumor cells can spread out of the primary tumors and enter the circulation. These circulating CX_3CR1^+ tumor cells are then easily attracted by any cellular source producing the ligand (endothelial/stromal cells of the bone marrow, brain) (51, 52).

In contrast, expression of the ligand has usually been associated with improved patient survival (26, 44, 53, 54). The antitumor effects of CX_3CL1 are mostly related to attraction of cytotoxic CD8 T lymphocytes and NK cells (40, 42, 43). However, CX_3CL1 may also stimulate tumor survival and proliferation, and in breast cancer it promotes tumor progression via *trans*-activation of the epidermal growth factor pathway (32, 52). The dual nature of the CX_3CR1-CX_3CL1 axis is an example of the complex interplay between neoplastic cells, the tumor stroma, and infiltrating leukocytes.

Historically, chemokines are viewed as mobilizing factors regulating cell trafficking in health and disease, and chemokine receptor expression by cancer cells was associated with tumor spreading (7, 55–57). It was therefore of interest, and indeed a novel finding in CRC, that the membrane-anchored ligand and the receptor are involved in tumor cell adhesion, acting as retention factors and preventing metastatic spread. Other examples of chemokines acting as retention factors are known. Most notable is the case of CXCR4 in hematopoietic stem cells, which are kept within the bone marrow niche by the ligand CXCL12; a similar situation occurs in immature thymocytes retained in the thymic cortex by the CXCR4-CXCL12 axis (58). Another chemokine–

receptor pair (CCL25-CCR9) was demonstrated to modulate colon cancer invasion and metastasis (59). CCL25 is expressed in the gastrointestinal microenvironment; when $CCR9^+$ human CRC cells were systemically injected in the blood of immune-deficient mice, they formed orthotopic tumors, whereas $CCR9^-$ cells formed only extraintestinal tumors, suggesting that CCL25 retained $CCR9^+$ neoplastic cells at primary tumor sites (59).

In conclusion, we have shown correlative clinical evidence that low or absent expression of the chemokine axis CX_3CL1-CX_3CR1 in human CRC identifies patients with higher risk of disease recurrence and formation of metachronous metastases. Our preclinical data are consistent with the view that the *trans*-membrane chemokine CX_3CL1 engages with its specific receptor in a strong adhesion loop that prevents tumor cell dissemination by holding locally CX_3CR1-positive cells.

Acknowledgments

We thank Dr. G. Vereb, University of Debrecen, Hungary, and Dr. A. Anselmo for initial experiments on integrin involvement in CX_3CR1-expressing cells; Dr. C. Buracchi and Dr. P. Somma for cell sorting; Dr. M. Fabbri, University of Varese, Italy, for informatics analysis; and Dr. M.L. Malosio for the lentiviral vector (21). We thank Dr. M. Kallikourdis for editing the manuscript.

Disclosures

The authors have no financial conflicts of interest.

References

1. Sadanandam, A., C. A. Lyssiotis, K. Homicsko, E. A. Collisson, W. J. Gibb, S. Wullschleger, L. C. Ostos, W. A. Lannon, C. Grotzinger, M. Del Rio, et al. 2013. A colorectal cancer classification system that associates cellular phenotype and responses to therapy. *Nat. Med.* 19: 619–625.
2. Celesti, G., G. Di Caro, P. Bianchi, F. Grizzi, G. Basso, F. Marchesi, A. Doni, G. Marra, M. Roncalli, A. Mantovani, A. Malesci, and L. Laghi. 2013. Presence of Twist1-positive neoplastic cells in the stroma of chromosome-unstable colorectal tumors. *Gastroenterology* 145: 647-657.e15.doi:10.1053/j.gastro.2013.05.011
3. Grivennikov, S. I., K. Wang, D. Mucida, C. A. Stewart, B. Schnabl, D. Jauch, K. Taniguchi, G. Y. Yu, C. H. Osterreicher, K. E. Hung, et al. 2012. Adenoma-linked barrier defects and microbial products drive IL-23/IL-17-mediated tumour growth. *Nature* 491: 254–258.
4. Jobin, C. 2013. Colorectal cancer: looking for answers in the microbiota. *Cancer Discov.* 3: 384–387.
5. Zambetti, L. P., and A. Mortellaro. 2014. NLRPs, microbiota, and gut homeostasis: unravelling the connection. *J. Pathol.* 233: 321–330.
6. Coussens, L. M., and Z. Werb. 2002. Inflammation and cancer. *Nature* 420: 860–867.
7. Mantovani, A., P. Allavena, A. Sica, and F. Balkwill. 2008. Cancer-related inflammation. *Nature* 454: 436–444.
8. Thun, M. J., E. J. Jacobs, and C. Patrono. 2012. The role of aspirin in cancer prevention. *Nat. Rev. Clin. Oncol.* 9: 259–267.
9. Grivennikov, S., E. Karin, J. Terzic, D. Mucida, G. Y. Yu, S. Vallabhapurapu, J. Scheller, S. Rose-John, H. Cheroutre, L. Eckmann, and M. Karin. 2009. IL-6 and Stat3 are required for survival of intestinal epithelial cells and development of colitis-associated cancer. *Cancer Cell* 15: 103–113.
10. Zaki, M. H., P. Vogel, R. K. Malireddi, M. Body-Malapel, P. K. Anand, J. Bertin, D. R. Green, M. Lamkanfi, and T. D. Kanneganti. 2011. The NOD-like receptor NLRP12 attenuates colon inflammation and tumorigenesis. *Cancer Cell* 20: 649–660.
11. Canna, K., P. A. McArdle, D. C. McMillan, A. M. McNicol, G. W. Smith, R. F. McKee, and C. S. McArdle. 2005. The relationship between tumour T-lymphocyte infiltration, the systemic inflammatory response and survival in patients undergoing curative resection for colorectal cancer. *Br. J. Cancer* 92: 651–654.
12. Laghi, L., P. Bianchi, E. Miranda, E. Balladore, V. Pacetti, F. Grizzi, P. Allavena, V. Torri, A. Repici, A. Santoro, et al. 2009. CD3+ cells at the invasive margin of deeply invading (pT3-T4) colorectal cancer and risk of post-surgical metastasis: a longitudinal study. *Lancet Oncol.* 10: 877–884.
13. Nosho, K., Y. Baba, N. Tanaka, K. Shima, M. Hayashi, J. A. Meyerhardt, E. Giovannucci, G. Dranoff, C. S. Fuchs, and S. Ogino. 2010. Tumour-infiltrating T-cell subsets, molecular changes in colorectal cancer, and prognosis: cohort study and literature review. *J. Pathol.* 222: 350–366.
14. Bindea, G., B. Mlecnik, M. Tosolini, A. Kirilovsky, M. Waldner, A. C. Obenauf, H. Angell, T. Fredriksen, L. Lafontaine, A. Berger, et al. 2013. Spatiotemporal dynamics of intratumoral immune cells reveal the immune landscape in human cancer. *Immunity* 39: 782–795.
15. Erreni, M., P. Bianchi, L. Laghi, M. Mirolo, M. Fabbri, M. Locati, A. Mantovani, and P. Allavena. 2009. Expression of chemokines and chemokine receptors in human colon cancer. *Methods Enzymol.* 460: 105–121.
16. Bazan, J. F., K. B. Bacon, G. Hardiman, W. Wang, K. Soo, D. Rossi, D. R. Greaves, A. Zlotnik, and T. J. Schall. 1997. A new class of membrane-bound chemokine with a CX3C motif. *Nature* 385: 640–644.
17. Garton, K. J., P. J. Gough, C. P. Blobel, G. Murphy, D. R. Greaves, P. J. Dempsey, and E. W. Raines. 2001. Tumor necrosis factor-alpha-converting enzyme (ADAM17) mediates the cleavage and shedding of fractalkine (CX3CL1). *J. Biol. Chem.* 276: 37993–38001.
18. Muehlhoefer, A., L. J. Saubermann, X. Gu, K. Luedtke-Heckenkamp, R. Xavier, R. S. Blumberg, D. K. Podolsky, R. P. MacDermott, and H. C. Reinecker. 2000. Fractalkine is an epithelial and endothelial cell-derived chemoattractant for intraepithelial lymphocytes in the small intestinal mucosa. *J. Immunol.* 164: 3368–3376.
19. D'Haese, J. G., I. E. Demir, H. Friess, and G. O. Ceyhan. 2010. Fractalkine/CX3CR1: why a single chemokine-receptor duo bears a major and unique therapeutic potential. *Expert Opin. Ther. Targets* 14: 207–219.
20. Jamieson, W. L., S. Shimizu, J. A. D'Ambrosio, O. Meucci, and A. Fatatis. 2008. CX3CR1 is expressed by prostate epithelial cells and androgens regulate the levels of CX3CL1/fractalkine in the bone marrow: potential role in prostate cancer bone tropism. *Cancer Res.* 68: 1715–1722.
21. Marchesi, F., L. Piemonti, G. Fedele, A. Destro, M. Roncalli, L. Albarello, C. Doglioni, A. Anselmo, A. Doni, P. Bianchi, et al. 2008. The chemokine receptor CX3CR1 is involved in the neural tropism and malignant behavior of pancreatic ductal adenocarcinoma. *Cancer Res.* 68: 9060–9069.
22. Erreni, M., G. Solinas, P. Brescia, D. Osti, F. Zunino, P. Colombo, A. Destro, M. Roncalli, A. Mantovani, R. Draghi, et al. 2010. Human glioblastoma tumours and neural cancer stem cells express the chemokine CX3CL1 and its receptor CX3CR1. *Eur. J. Cancer* 46: 3383–3392.
23. Celesti, G., G. Di Caro, P. Bianchi, F. Grizzi, F. Marchesi, G. Basso, D. Rahal, G. Delconte, M. Catalano, P. Cappello, et al. 2013. Early expression of the fractalkine receptor CX3CR1 in pancreatic carcinogenesis. *Br. J. Cancer* 109: 2424–2433.
24. Wei, L. M., S. Cao, W. D. Yu, Y. L. Liu, and J. T. Wang. 2015. Overexpression of CX3CR1 is associated with cellular metastasis, proliferation and survival in gastric cancer. *Oncol. Rep.* 33: 615–624.
25. Lavergne, E., B. Combadière, O. Bonduelle, M. Iga, J. L. Gao, M. Maho, A. Boissonnas, P. M. Murphy, P. Debré, and C. Combadière. 2003. Fractalkine mediates natural killer-dependent antitumor responses in vivo. *Cancer Res.* 63: 7468–7474.
26. Ohta, M., F. Tanaka, H. Yamaguchi, N. Sadanaga, H. Inoue, and M. Mori. 2005. The high expression of Fractalkine results in a better prognosis for colorectal cancer patients. *Int. J. Oncol.* 26: 41–47.
27. Sciumè, G., A. Soriani, M. Piccoli, L. Frati, A. Santoni, and G. Bernardini. 2010. CX3CR1/CX3CL1 axis negatively controls glioma cell invasion and is modulated by transforming growth factor-β1. *Neuro-oncol.* 12: 701–710.
28. Galon, J., A. Costes, F. Sanchez-Cabo, A. Kirilovsky, B. Mlecnik, C. Lagorce-Pagès, M. Tosolini, M. Camus, A. Berger, P. Wind, et al. 2006. Type, density, and location of immune cells within human colorectal tumors predict clinical outcome. *Science* 313: 1960–1964.
29. Ladoire, S., F. Martin, and F. Ghiringhelli. 2011. Prognostic role of FOXP3+ regulatory T cells infiltrating human carcinomas: the paradox of colorectal cancer. *Cancer Immunol. Immunother.* 60: 909–918.
30. Goda, S., T. Imai, O. Yoshie, O. Yoneda, H. Inoue, Y. Nagano, T. Okazaki, H. Imai, E. T. Bloom, N. Domae, and H. Umehara. 2000. CX3C-chemokine, fractalkine-enhanced adhesion of THP-1 cells to endothelial cells through integrin-dependent and -independent mechanisms. *J. Immunol.* 164: 4313–4320.
31. Lauro, C., M. Catalano, F. Trettel, F. Mainiero, M. T. Ciotti, F. Eusebi, and C. Limatola. 2006. The chemokine CX3CL1 reduces migration and increases adhesion of neurons with mechanisms dependent on the beta1 integrin subunit. *J. Immunol.* 177: 7599–7606.
32. Tardáguila, M., E. Mira, M. A. García-Cabezas, A. M. Feijoo, M. Quintela-Fandino, I. Azcoitia, S. A. Lira, and S. Mañes. 2013. CX3CL1 promotes breast cancer via transactivation of the EGF pathway. *Cancer Res.* 73: 4461–4473.
33. Digman, M. A., V. R. Caiolfa, M. Zamai, and E. Gratton. 2008. The phasor approach to fluorescence lifetime imaging analysis. *Biophys. J.* 94: L14–L16.
34. Lucas, A. D., N. Chadwick, B. F. Warren, D. P. Jewell, S. Gordon, F. Powrie, and D. R. Greaves. 2001. The transmembrane form of the CX3CL1 chemokine fractalkine is expressed predominantly by epithelial cells in vivo. *Am. J. Pathol.* 158: 855–866.
35. Shang, L., N. Thirunarayanan, A. Viejo-Borbolla, A. P. Martin, M. Bogunovic, F. Marchesi, J. C. Unkeless, Y. Ho, G. C. Furtado, A. Alcami, et al. 2009. Expression of the chemokine binding protein M3 promotes marked changes in the accumulation of specific leukocytes subsets within the intestine. *Gastroenterology* 137: 1006-1018, 1018.e1-3. doi:10.1053/j.gastro.2009.05.055
36. Trinchieri, G. 2014. Critical role for CX_3CR1^+ mononuclear phagocytes in intestinal homeostasis. *J. Exp. Med.* 211: 1500–1501.
37. Tsou, C. L., C. A. Haskell, and I. F. Charo. 2001. Tumor necrosis factor-alpha-converting enzyme mediates the inducible cleavage of fractalkine. *J. Biol. Chem.* 276: 44622–44626.
38. Calon, A., E. Espinet, S. Palomo-Ponce, D. V. Tauriello, M. Iglesias, M. V. Céspedes, M. Sevillano, C. Nadal, P. Jung, X. H. Zhang, et al. 2012. Dependency of colorectal cancer on a TGF-β-driven program in stromal cells for metastasis initiation. *Cancer Cell* 22: 571–584.

39. McCulloch, D. R., M. Harvey, and A. C. Herington. 2000. The expression of the ADAMs proteases in prostate cancer cell lines and their regulation by dihydrotestosterone. *Mol. Cell. Endocrinol.* 167: 11–21.
40. Vitale, S., B. Cambien, B. F. Karimdjee, R. Barthel, P. Staccini, C. Luci, V. Breittmayer, F. Anjuère, A. Schmid-Alliana, and H. Schmid-Antomarchi. 2007. Tissue-specific differential antitumour effect of molecular forms of fractalkine in a mouse model of metastatic colon cancer. *Gut* 56: 365–372.
41. Ostuni, M. A., J. Guellec, P. Hermand, P. Durand, C. Combadière, F. Pincet, and P. Deterre. 2014. CX3CL1, a chemokine finely tuned to adhesion: critical roles of the stalk glycosylation and the membrane domain. *Biol. Open* 3: 1173–1182.
42. Hyakudomi, M., T. Matsubara, R. Hyakudomi, T. Yamamoto, S. Kinugasa, A. Yamanoi, R. Maruyama, and T. Tanaka. 2008. Increased expression of fractalkine is correlated with a better prognosis and an increased number of both CD8+ T cells and natural killer cells in gastric adenocarcinoma. *Ann. Surg. Oncol.* 15: 1775–1782.
43. Park, M. H., J. S. Lee, and J. H. Yoon. 2012. High expression of CX3CL1 by tumor cells correlates with a good prognosis and increased tumor-infiltrating CD8+ T cells, natural killer cells, and dendritic cells in breast carcinoma. *J. Surg. Oncol.* 106: 386–392.
44. Mlecnik, B., M. Tosolini, P. Charoentong, A. Kirilovsky, G. Bindea, A. Berger, M. Camus, M. Gillard, P. Bruneval, W. H. Fridman, et al. 2010. Biomolecular network reconstruction identifies T-cell homing factors associated with survival in colorectal cancer. *Gastroenterology* 138: 1429–1440.
45. Halama, N., S. Michel, M. Kloor, I. Zoernig, A. Benner, A. Spille, T. Pommerencke, D. M. von Knebel, G. Folprecht, B. Luber, et al. 2011. Localization and density of immune cells in the invasive margin of human colorectal cancer liver metastases are prognostic for response to chemotherapy. *Cancer Res.* 71: 5670–5677.
46. Zheng, J., M. Yang, J. Shao, Y. Miao, J. Han, and J. Du. 2013. Chemokine receptor CX3CR1 contributes to macrophage survival in tumor metastasis. *Mol. Cancer* 12: 141.
47. Xiao, L. J., Y. Y. Chen, P. Lin, H. F. Zou, F. Lin, L. N. Zhao, D. Li, L. Guo, J. B. Tang, X. L. Zheng, and X. G. Yu. 2012. Hypoxia increases CX3CR1 expression via HIF-1 and NF-κB in androgen-independent prostate cancer cells. *Int. J. Oncol.* 41: 1827–1836.
48. Zhao, T., S. Gao, X. Wang, J. Liu, Y. Duan, Z. Yuan, J. Sheng, S. Li, F. Wang, M. Yu, et al. 2012. Hypoxia-inducible factor-1α regulates chemotactic migration of pancreatic ductal adenocarcinoma cells through directly transactivating the CX3CR1 gene. *PLoS One* 7: e43399.
49. Matsubara, T., T. Ono, A. Yamanoi, M. Tachibana, and N. Nagasue. 2007. Fractalkine-CX3CR1 axis regulates tumor cell cycle and deteriorates prognosis after radical resection for hepatocellular carcinoma. *J. Surg. Oncol.* 95: 241–249.
50. Jamieson-Gladney, W. L., Y. Zhang, A. M. Fong, O. Meucci, and A. Fatatis. 2011. The chemokine receptor CX$_3$CR1 is directly involved in the arrest of breast cancer cells to the skeleton. *Breast Cancer Res.* 13: R91.
51. Nevo, I., O. Sagi-Assif, T. Meshel, A. Ben-Baruch, K. Jöhrer, R. Greil, L. E. Trejo, O. Kharenko, M. Feinmesser, I. Yron, and I. P. Witz. 2009. The involvement of the fractalkine receptor in the transmigration of neuroblastoma cells through bone-marrow endothelial cells. *Cancer Lett.* 273: 127–139.
52. Ferretti, E., V. Pistoia, and A. Corcione. 2014. Role of fractalkine/CX3CL1 and its receptor in the pathogenesis of inflammatory and malignant diseases with emphasis on B cell malignancies. *Mediators Inflamm.* DOI: 10.1155/2014/480941.
53. Kehlen, A., T. Greither, S. Wach, E. Nolte, M. Kappler, M. Bache, H. J. Holzhausen, C. Lautenschläger, S. Göbel, P. Würl, et al. 2014. High coexpression of CCL2 and CX3CL1 is gender-specifically associated with good prognosis in soft tissue sarcoma patients. *Int. J. Cancer* 135: 2096–2106.
54. Tardáguila, M., and S. Mañes. The complex role of chemokines in cancer: the case of the CX3CL1/CX3CR1 axis. *Oncology Theory & Practice*
55. Balkwill, F. 2004. Cancer and the chemokine network. *Nat. Rev. Cancer* 4: 540–550.
56. Mantovani, A., B. Savino, M. Locati, L. Zammataro, P. Allavena, and R. Bonecchi. 2010. The chemokine system in cancer biology and therapy. *Cytokine Growth Factor Rev.* 21: 27–39.
57. Zlotnik, A., A. M. Burkhardt, and B. Homey. 2011. Homeostatic chemokine receptors and organ-specific metastasis. *Nat. Rev. Immunol.* 11: 597–606.
58. Halkias, J., H. J. Melichar, K. T. Taylor, J. O. Ross, B. Yen, S. B. Cooper, A. Winoto, and E. A. Robey. 2013. Opposing chemokine gradients control human thymocyte migration in situ. *J. Clin. Invest.* 123: 2131–2142.
59. Chen, H. J., R. Edwards, S. Tucci, P. Bu, J. Milsom, S. Lee, W. Edelmann, Z. H. Gümüs, X. Shen, and S. Lipkin. 2012. Chemokine 25-induced signaling suppresses colon cancer invasion and metastasis. *J. Clin. Invest.* 122: 3184–3196.